

# MR quantitative 3D shape analysis helps to distinguish mucinous cystic neoplasm from serous oligocystic adenoma

Shuo Zhu   
Wen-Tao Wang   
Wen-Chuan Wu   
Wen-Hui Lou   
Meng-Su Zeng   
Sheng-Xiang Rao 

## PURPOSE

We aimed to assess the performance of quantitative 3D shape analysis in the differential diagnosis of pancreatic serous oligocystic adenoma (SOA) and mucinous cystic neoplasm (MCN).

## METHODS

Four hundred thirty-two patients diagnosed with serous cystic neoplasms (SCNs) or MCNs were retrospectively reviewed from August 2014 to July 2019 and finally 87 patients with MCNs (n = 45) and SOAs (n = 42) were included. Clinical data and magnetic resonance morphologic features with 3D shape analysis of lesions (shape sphericity, compacity, and volume) were recorded and compared between MCNs and SOAs according to the pathology. Univariable and multivariable regression analyses were used to identify independent impact factors for differentiating MCN from SOA.

## RESULTS

The age of MCN patients was younger than SOAs ( $43.02 \pm 10.83$  years vs.  $52.78 \pm 12.31$  years; OR = 0.275; 95% CI: 0.098-0.768;  $P = .014$ ). MCN has a higher female/male ratio than SOA (43/2 vs. 27/15; OR = 40.418; 95% CI: 2.704-604.171;  $P = .007$ ) and was more often located in the distal of pancreas (OR = 31.403; 95% CI: 2.985-330.342;  $P = .004$ ). Shape\_Sphericity derived from 3D shape analysis was a significant independent factor in the multivariable analysis and the value of MCN was closer to 1 than SOA (OR = 35.153; 95% CI: 5.301-237.585;  $P < .001$ ). Area under the receiver operating characteristic curve (AUC) of Shape\_Sphericity was 0.923 (optimal cutoff value was 0.964876).

## CONCLUSION

Shape\_Sphericity in combination with age, sex, and location could help to distinguish MCN from SOA.

Given the advances and expanding use of image examination, more and more pancreatic cystic lesions (PCLs) are being identified by accident. The diagnostic prevalence of PCLs was reported between 2.4% and 49.1% for different detecting modalities, and magnetic resonance imaging (MRI) outperformed computed tomography (CT) for detecting PCLs and providing additional preoperative information on surgical resection.<sup>1-8</sup> PCLs consist of numerous pathological types and a part of cystic pancreatic neoplasms has potential malignant transformation. Serous cystadenoma and pseudocysts have scarce potential of malignancy, whereas mucinous cystic neoplasms (MCNs) and intraductal papillary mucinous neoplasms are considered to have malignant potential. Goh et al. reported that PCLs can be assumed to be malignant in about 31% and potentially malignant in 29% of cases, which required differentiated management.<sup>9</sup> Although the knowledge of the pathological and radiological characteristics of PCLs has broadened considerably, the accuracy of conventional imaging features used to distinguish serous cystadenoma (SCA) and mucinous cystadenoma (MCA) is still unsatisfactory. It has been reported that blind reviewers may correctly identify above 90% of MCAs or SCAs, whereas another research showed that SCA and MCA are correctly distinguished in only 27% and 25%.<sup>10,11</sup>

From the Department of Radiology (S.Z., W.-T.W., M.-S.Z., S.-X.R. ✉ raoxray@163.com), Fudan University, and Shanghai Institute of Medical Imaging, Shanghai, China Department of General Surgery (W.-C.W., W.-H.L.), Zhongshan Hospital, Fudan University, Shanghai, China.

Received 8 October 2020; revision requested 23 November; last revision received 19 March; accepted 1 April 2021.

DOI: 10.5152/dir.2022.20738

You may cite this article as: Zhu S, Wang W, Wu W, Lou W, Zeng M, Rao S. MR quantitative 3D shape analysis helps to distinguish mucinous cystic neoplasm from serous oligocystic adenoma. *Diagn Interv Radiol.* 2022;28(3):193-199.

Since Lewandrowski et al. reported that macrocystic SOA could present as a unilocular lesion, many researches have revealed that some serous oligocystic adenoma (SOA) were misdiagnosed as other cystic lesions of the pancreas, which were treated inappropriately.<sup>12-20</sup> It is essential to make an accurate diagnosis to allow subsequent decisions. Unnecessary surgery for SOA should be avoided because it is always benign, but MCN should be considered to know whether surgical resection is needed.<sup>18,21</sup> Typical cases such as a typical serous cystic neoplasm (SCN) with a distinctive central stellate scar could be correctly diagnosed by routine images, but only about 20% of the tumors have this feature.<sup>19</sup> It is difficult to distinguish SOA, especially oligocystic types, from mucinous cystadenoma based on images.<sup>22,23</sup>

In the past, quantitative three-dimensional (3D) shape analysis of medical images was approached with more interest, since it provided a reproducible and particular quantitative assessment of morphology. Some studies have reported that the 3D shape parameters obtained from the lesions could help to discriminate risk level of different tumors, such as thymoma and gastrointestinal stromal tumors, among others.<sup>24,25</sup> However, to our knowledge, no study to date attempted to identify serous macrocystic adenoma and mucinous cystadenoma by computerized 3D shape analysis, especially using MRI, which can show more internal details of lesions than CT. We evaluated the morphological features and 3D shape analysis to distinguish SOA from MCA.

## Methods

This retrospective research was approved by the Ethics Committee at Zhongshan Hospital of Fudan University and written

### Main points

- It is difficult to distinguish serous oligocystic adenomas (SOA) and mucinous cystic neoplasms (MCN) before surgery by routine imaging.
- SOA is often treated by unnecessary surgery, even though it has a scarce potential of malignancy.
- Shape\_Sphericity in combination with age, sex, and location played an important role in differentiating MCN from SOA.

informed consent was waived. The decision number was B2014-019.

### Study subjects

From August 2014 to July 2019, 321 consecutive patients with a pathologic diagnosis of MCNs SCNs were identified at our institution. The inclusion criteria of the study were: (a) preoperative contrast-enhanced MRI examination with magnetic resonance cholangiopancreatography (MRCP), (b) less than 4 weeks between MRI examination and surgical resection, and (c) lesions diagnosed as MCN and SCN by histopathology. The exclusion criteria were: (a) preoperative MRI examinations in other hospitals (n=76), (b) use of CT or unenhanced MRI for preoperative examination (n=84), (c) diagnosed as SCN rather than SOA (n=46), (d) unqualified MR images such as breathing artifact (n=13), and (e) more than 4 weeks between MRI and surgery (n=15). Finally, 45 patients with MCN and 42 patients with SOA were enrolled. Figure 1 shows the flowchart of this study.

### Magnetic resonance imaging acquisition

All abdominal examinations were performed using 1.5T MRI scanners (Avanto and Aera; Siemens Healthcare). The sequences of our protocols were (1) axial T2-weighted turbo spin-echo sequence; (2) axial T1-weighted sequence with in- and out-of-phase; (3) diffusion-weighted imaging (b=0, 50, 500 s/mm<sup>2</sup>) sequence with a free-breathing technique. Corresponding apparent

diffusion coefficient maps were also needed; (4) coronal T2-weighted MRCP; (5) post-contrast images of dynamic T1-weighted examination including arterial (20-30 s), portal venous (70-80 s), and delayed phases (180 s) obtained after a 0.2 mL/kg bolus injection of gadopentetate dimeglumine (Magnevist, Bayer HealthCare) at a speed of 2 mL/s. Parameters of MRI sequences are summarized in Table 1.

### 3D shape analysis

Obtained MR images were copied to a computer for analysis. 3D shape analysis was extracted from enhanced-MR images by using LIFEX software, which can be accessed through the website (<http://www.lifexsoft.org>).<sup>26</sup> Two board-certified radiologists with 5 years and 13 years of abdominal diagnosis experience (reader 1 and 2) subsequently contoured images of the cysts by the software and intraclass correlation coefficient (ICC) was calculated. Both readers only had images and were unaware of pathological and clinical information. Region of interest was drawn manually on every image until the entire lesion was included. Then 3 quantitative 3D shape parameters were calculated: (1) sphericity: how spherical a volume of interest is, which ranges from 0 to 1. If sphericity is closer to 1, then the shape is closer to a sphere, (2) compacity: reflecting how compact the volume of interest is, and (3) volume (voxels): the volume of interest in voxels. The 3D shape parameter formulas are shown as follows:

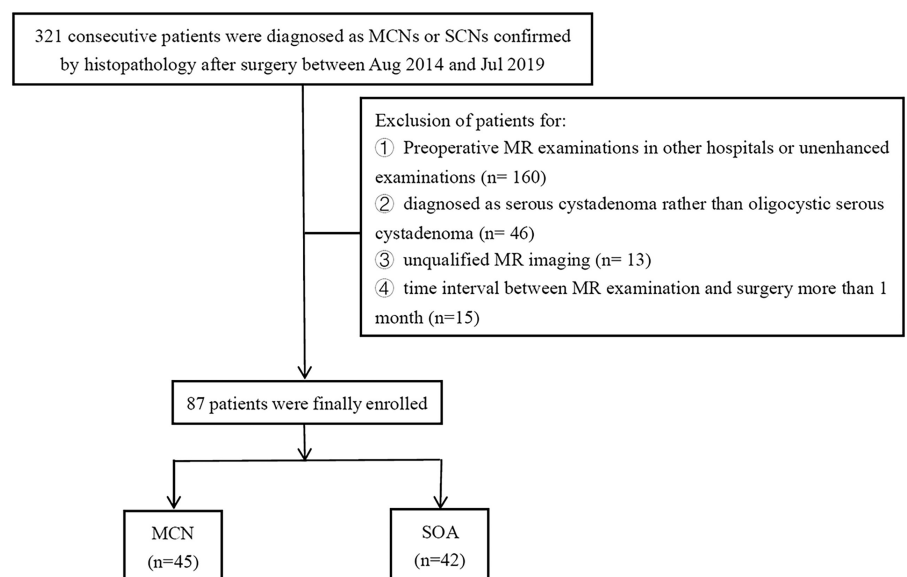


**Figure 1.** The flow diagram shows inclusion and exclusion criteria for the study. MCN, mucinous cystic neoplasm; SCN, serous cystic neoplasm; MR, magnetic resonance; SOA, serous oligocystic adenoma.

**Table 1.** MRI acquisition parameters

Sequence	Area 1.5T			Avanto 1.5T		
	TSE T2WI	DWI	3D GRE T1WI	TSE T2WI	DWI	3D GRE T1WI
Repetition time (ms)	3500	3200	4.38	3300	2400-2600	5.04
Echo time (ms)	84	56	1.93	70	66	2.31
Matrix size	194 × 256	84 × 128	216 × 288	207 × 384	112 × 128	250 × 512
Field of view (mm <sup>2</sup> )	360 × 360	380-400 × 300-324	380-400 × 300-324	330 × 330 to 380 × 380	330 × 330 to 380 × 380	330 × 330 to 380 × 380
Slice thickness (mm)	5	5.5	3	5	7	3

TSE T2WI, turbo spin-echo T2-weighted imaging; DWI, diffusion-weighted imaging; 3D GRE T1WI, 3-dimensional gradient recalled echo T1-weighted imaging.

$$1. \text{SHAPE\_Sphericity} = \frac{\frac{1}{\pi^3} \cdot (6 \cdot \text{Volume})^{2/3}}{A}$$

where V and A correspond to the volume and the surface of the volume of interest based on the Delaunay triangulation.

$$2. \text{SHAPE\_Compacity} = \frac{A^{3/2}}{V}$$

where V and A correspond to the volume and the surface of the volume of interest based on the Delaunay triangulation.

$$3. \text{SHAPE\_Volume (mL and voxels)} = \sum_i V_i$$

where  $V_i$  corresponds to volume voxel  $i$  of the volume of interest.

Detailed explanations can be found in the Texture-Guide on the LIFXE website. An example of contouring of mucinous cystadenomas on MR images is shown in Figure 2.

### Clinical and morphologic features analysis

The following series of clinical data were collected: age, sex, symptom, and the time interval between MRI examination and surgery. Radiologists also evaluated the following features of images: the maximum

diameter of the lesion, locations, morphology (round or oval and lobulation), and the presence of septa. If there was any disagreement between reader 1 and 2, another experienced abdominal radiologist made the final decision. For multiple lesions, only the largest was recorded. A lesion was considered to be lobulated if it had the shape of a closed curve with smooth and multiple external undulations.<sup>27</sup>

### Statistical analysis

Normal distribution was determined by the Kolmogorov–Smirnov test. Descriptive statistics of the data are presented with n (%) and normal distributions are shown as mean ± standard deviation (SD). An independent t test was used to compare normally distributed variables and the Pearson chi-square test was used to compare categorical variables. Univariable and multivariable logistic regression analyses were performed using the backward method. Wald was performed to statistically assess the difference and discriminate performance between SOAs and MCNs. All the continuous parameters in univariate or multivariate analyses

were expressed as the mean values from the 2 observers and transformed into z score normalization to reduce the bias caused by different dimensions. Factors with a *P* value of .10 or less at univariate analyses were included in the multivariable model. Odds ratios and 95% CIs were calculated. Receiver operating characteristic (ROC) curve and area under the ROC curve with 95% CIs were calculated for the continuous variables which were statistically significant at multivariable analysis. The corresponding sensitivity and specificity values and the optimal cutoff value were calculated. A two-sided *P* value of less than .05 was considered indicative of a significant difference. All statistical analyses were conducted in Statistical Package for the Social Sciences software (version 24.0, IBM).

## Results

Among the 321 patients, 87 patients (mean age: 47.74 ± 12.51 years) including 19.54% (17/87) men (49.35 ± 13.98 years) and 80.46% (70/87) women (47.34 ± 12.20 years) were finally enrolled, with SOAs (*n* = 42) and MCNs (*n* = 45) according to the pathology. Of the patients, 37.93% (33/87) had symptoms at initial diagnostic time. Around 51.11% (23/45) of patients with MCNs and 61.90% (13/42) of patients with SOAs had symptoms such as abdominal pain or abdominal distension, but there was no significant difference (OR = 1.785; 95% CI: 0.741-4.301; *P* = .197). The mean age of MCNs patients was less than SOAs (43.02 ± 10.83 years vs. 52.78 ± 12.31 years; OR = 0.576; 95% CI: 0.365-0.908; *P* = .018). There were 2 males in the MCNs population and 15 males in the SOAs, which had statistical significance (OR = 11.944; 95% CI: 2.530-56.384; *P* = .002).

The morphological characteristics were imported from MR images, including

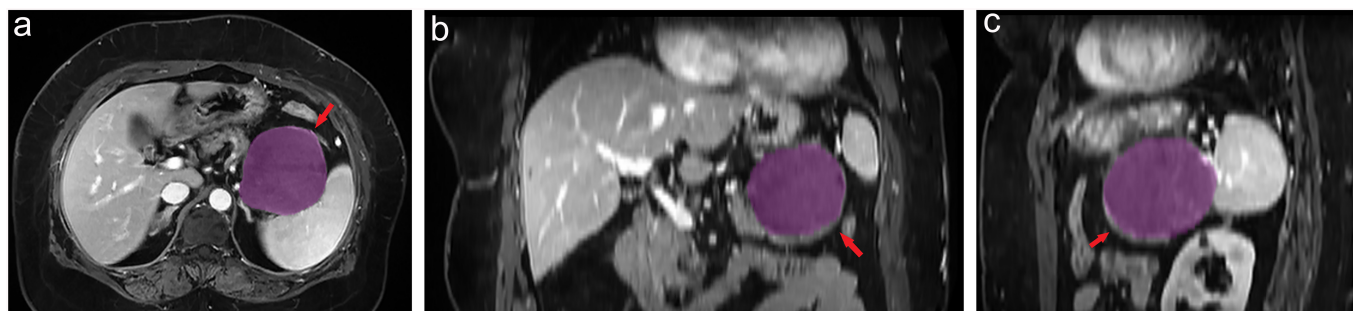


**Figure 2. a-c.** A 61-year-old woman with a mucinous cystadenoma. Example of semiautomatic contouring of mucinous cystadenomas on MR images. (a) When a reader manually created ROIs (the area filled with purple) on consecutive MRI slices, the software automatically generated ROIs of coronal and sagittal slices (b and c). In cases in which ROIs automatically generated by the software were not sufficiently accurate, readers could manually modify them.

maximum diameter, location, morphology, and septum. Among 87 patients, the mean diameter of lesions was  $39.85 \pm 21.79$  mm. The mean diameter of MCNs was larger than that of SOAs ( $45.69 \pm 26.60$  vs.  $33.60 \pm 12.61$  mm; OR=1.031; 95% CI: 1.006-1.058;  $P=.015$ ). About 88.89% (40/47) of MCNs were in the distal pancreas (pancreatic body and tail), compared to 57.14% (24/42) of SOAs (OR=6.00; 95% CI: 1.972-18.253;  $P=.002$ ). Regarding tumor contour, MCNs were more smooth than SOAs (82.22% vs. 17.78%, OR=0.068; 95% CI: 0.024-0.192;  $P < .001$ ).

Regarding the quantitative variables of the lesions extracted from MRI, the mean SHAPE\_Volume (# vx) of MCNs was  $36\ 395.76 \pm 52\ 275.67$ , compared to  $17\ 128.07 \pm 19\ 224.72$  in SOAs (OR=2.424; 95% CI: 1.036-5.671;  $P=.041$ ), but no significant difference was found after multivariate analysis. The mean SHAPE\_Sphericity of MCNs was also higher than SOAs ( $0.979977 \pm 0.12$  vs.  $0.950264 \pm 0.18$ , OR=19.973; 95% CI: 5.939-67.170;  $P < .001$ ). No significant difference was found in Shape\_Compacity between MCNs and SOAs. The ICC of SHAPE\_Volume (# vx), SHAPE\_Sphericity, and Shape\_Compacity between reader 1 and 2 were 0.905, 0.883, and 0.892 ( $P < .001$ ), respectively.

Age, sex, location, SHAPE\_Volume, and SHAPE\_Sphericity were entered into

the multivariate model after univariate analyses. Age was still a significant factor for differentiating MCN from SOA (OR=0.275; 95% CI: 0.098-0.768;  $P=.014$ ). MCN has a higher female/male ratio than SOA (OR=40.418; 95% CI: 2.704-604.171;  $P=.007$ ) and is more frequently located in the distal pancreas (OR=31.403; 95% CI: 2.985-330.342;  $P=.004$ ). Shape\_Sphericity was the only significant factor in 3D shape analysis and the value of MCN was closer to 1 than SOA (OR=35.153; 95% CI: 5.301-237.585;  $P < .001$ ). They indicate the  $P$  value regarding the significance of the model to be  $<.05$  and adjusted R square value to be 0.600. Baseline characteristics of patient population and conventional MRI findings are summarized in Tables 2 and 3. Samples of MCN and SOA are presented in Figures 3 and 4. The area under the ROC curve (AUC) of age, sex, location, and Shape\_Sphericity was 0.270 (95% CI: 0.165, 0.376), 0.656 (95% CI: 0.540, 0.773), 0.659 (95% CI: 0.542, 0.775), and 0.923 (95% CI: 0.864, 0.982), the  $P$  values were  $<.001$ , .012, .011, and  $<.001$ , respectively. The AUC of Shape\_Sphericity was highest and the optimal cutoff value of Shape\_Sphericity was 0.964876 and the sensitivity and specificity were 91.1% and 88.1%, respectively. The result is shown in Table 4 and Figure 5.

## Discussion

The routine examination to distinguish SCA and MCA is still unsatisfactory. This study aimed to use new technology to explore more imaging features to improve clinical diagnosis accuracy. Due to the different biological characteristics between MCNs and SOAs, the current guidelines usually recommend resection for MCNs but not for SOAs.<sup>28,29</sup> So making an accurate diagnosis before surgery is essential to avoid or minimize inappropriate surgical resection, and decide which mucinous cystadenoma requires surgical resection.<sup>18,21</sup> However, it is difficult to distinguish serous cystadenoma, especially oligocystic types, from mucinous cystadenoma by noninvasive imaging methods.<sup>22,23</sup>

This study evaluated the differences between the MCNs and SOAs by morphological features and 3D shape analysis. The results suggest age, location, sex, and Shape\_Sphericity as important features for differentiating MCNs from SOAs. The factors associated with MCNs were older female patients and lesions located at the distal pancreas (body and tail) and the Shape\_Sphericity was closer to 1.

Studies reported that the incidence of serous cystadenoma is about 10% and women (>65%) are detected with more frequency, with a peak age of 65 years. According to the classification of the World Health Organization, SOA as a subgroup of SCA is equal to macrocystic serous cystadenoma.<sup>12,30</sup> Moreover, the incidence of mucinous cystadenoma is about 8%; MCNs occur mostly in women aged between 42 and 60 years, with a potential of malignant transformation.<sup>31</sup> In this study, we found that patients with MCNs were younger than SOAs ( $43.02 \pm 10.83$  vs.  $52.78 \pm 12.31$ ), which was in accordance with the previous studies.

To date, several reports suggested that location and sex could help us to differentiate MCNs from SOAs. We found that more MCNs located in the distal pancreas, compared to SOAs. At the same time, we found that mucinous cystadenoma has a higher female/male ratio than serous cystadenoma (43/2 vs. 27/15). One theory is that the MCN has an ovarian stroma.<sup>15</sup> Another theory suggests that the female hormones stimulate the immature stroma or that the dorsal pancreas is affected because of being near the genital tract during

**Table 2.** Characteristics of patients and SOAs and MCNs detected by MRI from 2014 to 2019

Characteristics	
Age (years), mean $\pm$ SD	47.74 $\pm$ 12.51
Sex (M/F), n (%)	17 (19.54%)/70(80.46%)
Maximum diameter (mm), mean $\pm$ SD	39.85 $\pm$ 21.79
Location, n (%)	
Head and neck	23 (26.44%)
Body and tail	64 (73.56%)
Symptom, n (%)	
Presence	33 (37.93%)
Absence	54 (62.07%)
Morphology, n (%)	
Rounded	47 (54.02%)
Lobulated	40 (45.98%)
Septa, n (%)	
Presence	49 (56.32%)
Absence	38 (43.68%)
Time interval between MRI examination and surgery (days), mean $\pm$ SD	8.45 $\pm$ 6.79
M/F, male/female.	

**Table 3.** Results of univariate and multivariate analyses of risk factors for MCNs versus SOAs

Parameter	MCN (n = 45)	SOA (n = 42)	P	MCN vs. SOA			
				Univariate analysis		Multivariable analysis	
				Odds ratio (95% CI)	P	Odds ratio	P
Age (years), mean ± SD	43.02 ± 10.83	52.78 ± 12.31	<.001	0.576 (0.365, 0.908)	.018	0.275 (0.098, 0.768)	.014
No. of male patients	2 (4.44%)	15 (35.71%)	<.001	11.944 (2.530, 56.384)	.002	40.418 (2.704, 604.171)	.007
Symptom			.195				
Presence	20 (44.44%)	13 (30.95%)		1.785 (0.741, 4.301)	.197		
Absence	25 (55.56%)	29 (69.05%)					
MRI findings							
Location			.022				
Head and neck	5 (11.11%)	13 (42.86%)					
Body and tail	40 (88.89%)	29 (57.14%)		3.586 (1.151, 11.177)	.028	31.403 (2.985, 330.342)	.004
Septa			.310		.311		
Presence	23 (51.11%)	26 (61.90%)		0.643 (0.274, 1.511)			
Absence	22 (48.89%)	16 (38.10%)					
SHAPE_Volume (# vx), mean ± SD	36 395.76 ± 52 275.67	17 128.07 ± 19 224.72	.030	2.424 (1.036, 5.671)	.041		
SHAPE_Sphericity (only for 3D ROI (nz > 1), mean ± SD	0.979977 ± 0.12	0.950264 ± 0.18	<.001	19.973 (5.939, 67.170)	<.001	35.153 (5.201, 237.585)	<.001
SHAPE_Compacity only for 3D ROI (nz > 1), mean ± SD	5.94 ± 2.61	5.09 ± 1.73	.073	1.507 (0.949, 2.394)	.083		

P value for the significance of the model was <.05 and adjusted R square value was 0.600. MCN, mucinous cystic neoplasm; SOA, serous oligocystic adenoma; SD, standard deviation.

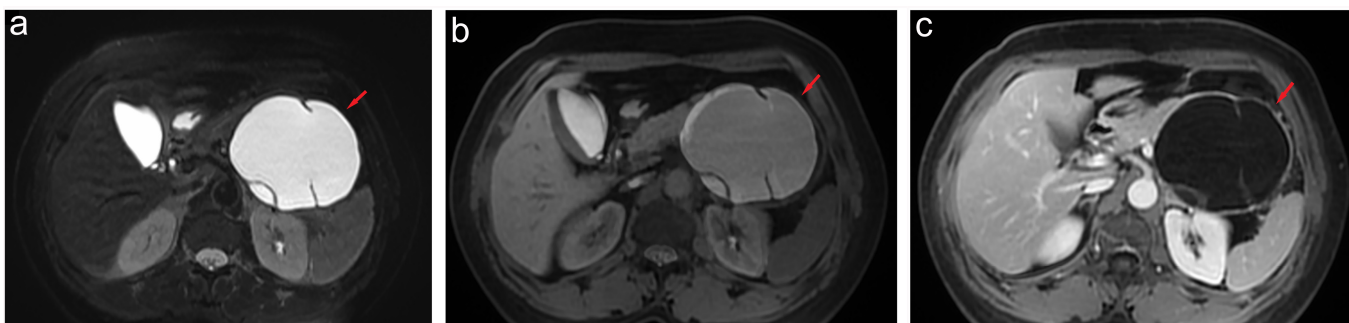


**Figure 3. a-c.** Images of a 46-year-old woman with a large mucinous cystadenoma located in the body and tail of the pancreas. Transverse T2-weighted fat-suppressed TSE MR image (**a**) shows one large rounded cystic lesion with well-defined and homogeneous high signal intensity (*arrow*). Several low signal intensity separations were shown within the lesion. Axial T1-weighted image (**b**) and venous phase image (**c**) show the low signal intensity of lesion and cyst wall and separations were slightly strengthened. The value of Shape\_Sphericity was 0.9925. TSE, turbo spin-echo; MR, magnetic resonance.



**Figure 4. a-c.** Images of a 70-year-old woman with a serious oligocystic adenoma confirmed by pathology located in the head of the pancreas. Transverse T2-weighted fat-suppressed TSE MR image (**a**) shows one large lobulated cystic lesion with well-defined and homogeneous high signal intensity (*arrow*). Several low signal intensity separations were shown within the lesion. Axial T1-weighted image (**b**) and venous phase image (**c**) show the low signal intensity of lesion and cyst wall and separations were slightly strengthened. The value of Shape\_Sphericity was 0.9285. TSE, turbo spin-echo; MR, magnetic resonance.

**Table 4.** Diagnostic performance of significant features for predicting MCNs

Features	Sensitivity	Specificity	Accuracy	PPV	NPV
Age (<21.5 years)	0 (0/45)	97.62% (41/42)	47.12% (41/87)	0 (0/1)	47.67% (41/86)
Sex (Female)	95.74% (45/47)	35.71% (15/42)	68.97% (60/87)	62.50% (45/72)	88.24% (15/17)
Location (body and tail)	88.89% (40/45)	30.95% (13/42)	60.92% (53/87)	57.97% (40/69)	72.22% (13/18)
SHAPE_Sphericity (>0.964876)	91.11% (41/45)	88.10% (37/42)	89.66% (78/87)	89.13% (41/46)	90.24% (37/41)

PPV, positive predictive value; NPV, negative predictive value.

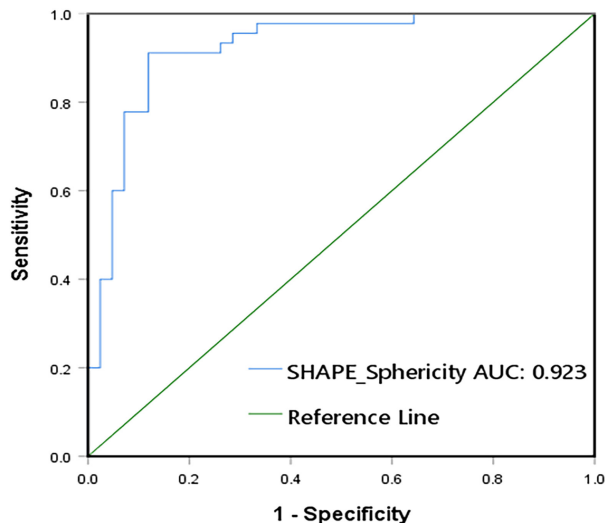


**Figure 5.** The graph shows the utility of the receiver operating characteristic curve of Shape\_Sphericity to discriminate SOAs and MCNs. The AUC of Shape\_Sphericity was 0.923 (95% CI: 0.864, 0.982) with the optimal Shape\_Sphericity cutoff value of 0.964876. SOA, serous oligocystic adenoma; MCN, mucinous cystic neoplasm; AUC, area under the receiver operating characteristic curve.

embryogenesis.<sup>32,33</sup> This result concurred with previous finding.<sup>22</sup>

In the past, many studies have reported that the textural parameters obtained from lesions can be used to discriminate between benign and malignant tumors in different organs.<sup>34-37</sup> In this study, the advantage of quantitative 3D shape analysis is that it provided more detailed information on morphology from images. The degree of lobulation could be quantitatively evaluated and it could assess the best cutoff value for distinguishing MCAs from SOAs. Some researchers have reported that the morphology of lesions was the most useful feature to differentiate SOA from MCA.<sup>22</sup> They found that lobulated shape was more common in SOA, but smooth shapes were more common in MCN. This is consistent with our research.

This study has several limitations. First, this study was retrospective and the number of patients was small, so we did not use texture analysis or radiomics analysis. This

limitation is currently unavoidable to some extent, and subsequent large-sample and multi-center studies need to be carried out. Second, we used 2 MR scanners, but at the same thickness (3 mm) which has limited affection on the 3D shape analysis. Moreover, whether the novel results could be transferred to 3.0T scanners are doubtful and we will include more samples to verify this result. Third, there are still a few subjective errors when drawing the region of interest of the lesion.

In conclusion, our results suggest that age, sex, location, and Shape\_Sphericity were important features for differentiating MCNs from SOAs. 3D shape analysis could provide a reproducible and quantitative assessment of morphology.

#### Financial disclosure

This research was supported by the National Key Research and Development Program of China (grant no: 2017YFC0108804).

#### Conflict of interest disclosure

The authors declared no conflicts of interest.

#### References

- de Jong K, Nio CY, Hermans JJ, et al. High prevalence of pancreatic cysts detected by screening magnetic resonance imaging examinations. *Clin Gastroenterol Hepatol.* 2010;8(9):806-811. [CrossRef]
- Lee KS, Sekhar A, Rofsky NM, Pedrosa I. Prevalence of incidental pancreatic cysts in the adult population on MR imaging. *Am J Gastroenterol.* 2010;105(9):2079-2084. [CrossRef]
- Laffan TA, Horton KM, Klein AP, et al. Prevalence of unsuspected pancreatic cysts on MDCT. *AJR Am J Roentgenol.* 2008;191(3):802-807. [CrossRef]
- Zhang XM, Mitchell DG, Dohke M, Holland GA, Parker L. Pancreatic cysts: depiction on single-shot fast spin-echo MR images. *Radiology.* 2002;223(2):547-553. [CrossRef]
- Martínez B, Martínez JF, Aparicio JR. Prevalence of incidental pancreatic cyst on upper endoscopic ultrasound. *Ann Gastroenterol.* 2018;31(1):90-95. [CrossRef]
- Moris M, Bridges MD, Pooley RA, et al. Association Between advances in high-resolution cross-section imaging technologies and increase in prevalence of pancreatic cysts from 2005 to 2014. *Clin Gastroenterol Hepatol.* 2016;14(4):e583. [CrossRef]
- Kromrey ML, Bülow R, Hübner J, et al. Prospective study on the incidence, prevalence and 5-year pancreatic-related mortality of pancreatic cysts in a population-based study. *Gut.* 2018;67(1):138-145. [CrossRef]
- Zhu S, Wang WT, Shang XS, et al. Difference analysis in prevalence of incidental pancreatic cystic lesions between computed tomography and magnetic resonance imaging. *BMC Med Imaging.* 2019;19(1):43. [CrossRef]
- Goh BK, Tan YM, Thng CH, et al. How useful are clinical, biochemical, and cross-sectional imaging features in predicting potentially malignant or malignant cystic lesions of the pancreas? Results from a single institution experience with 220 surgically treated patients. *J Am Coll Surg.* 2008;206(1):17-27. [CrossRef]
- Curry CA, Eng J, Horton KM, et al. CT of primary cystic pancreatic neoplasms: can CT be used for patient triage and treatment? *AJR Am J Roentgenol.* 2000;175(1):99-103. [CrossRef]
- Johnson CD, Stephens DH, Charboneau JW, Carpenter HA, Welch TJ. Cystic pancreatic tumors: CT and sonographic assessment. *AJR Am J Roentgenol.* 1988;151(6):1133-1138. [CrossRef]
- Lewandrowski K, Warsaw A, Compton C. Macrocystic serous cystadenoma of the pancreas: a morphologic variant differing from microcystic adenoma. *Hum Pathol.* 1992;23(8):871-875. [CrossRef]
- Warsaw AL, Compton CC, Lewandrowski K, Cardenosa G, Mueller PR. Cystic tumors of the pancreas. New clinical, radiologic, and pathologic observations in 67 patients. *Ann Surg.* 1990;212(4):432-435. [CrossRef]
- Warsaw AL, Rutledge PL. Cystic tumors mistaken for pancreatic pseudocysts. *Ann Surg.* 1987;205(4):393-398. [CrossRef]

15. Martin I, Hammond P, Scott J, Redhead D, Carter DC, Garden OJ. Cystic tumours of the pancreas. *Br J Surg*. 1998;85(11):1484-1486. [\[CrossRef\]](#)
16. Procacci C, Graziani R, Bicego E, et al. Serous cystadenoma of the pancreas: report of 30 cases with emphasis on the imaging findings. *J Comput Assist Tomogr*. 1997;21(3):373-382. [\[CrossRef\]](#)
17. Talamini MA, Pitt HA, Hruban RH, Boitnott JK, Coleman J, Cameron JL. Spectrum of cystic tumors of the pancreas. *Am J Surg*. 1992;163(1):117-123. [\[CrossRef\]](#)
18. Pyke CM, van Heerden JA, Colby TV, Sarr MG, Weaver AL. The spectrum of serous cystadenoma of the pancreas. Clinical, pathologic, and surgical aspects. *Ann Surg*. 1992;215(2):132-139. [\[CrossRef\]](#)
19. Le Borgne J, de Calan L, Partensky C. Cystadenomas and cystadenocarcinomas of the pancreas: a multiinstitutional retrospective study of 398 cases. French Surgical Association. *Ann Surg*. 1999;230(2):152-161. [\[CrossRef\]](#)
20. Ooi LL, Ho GH, Chew SP, Low CH, Soo KC. Cystic tumours of the pancreas: a diagnostic dilemma. *Aust N Z J Surg*. 1998;68(12):844-846. [\[CrossRef\]](#)
21. Ketwaroo GA, Morteale KJ, Sawhney MS. Pancreatic cystic neoplasms: an update. *Gastroenterol Clin North Am*. 2016;45(1):67-81. [\[CrossRef\]](#)
22. Kim SY, Lee JM, Kim SH, et al. Macrocystic neoplasms of the pancreas: CT differentiation of serous oligocystic adenoma from mucinous cystadenoma and intraductal papillary mucinous tumor. *AJR Am J Roentgenol*. 2006;187(5):1192-1198. [\[CrossRef\]](#)
23. Goh BK, Tan YM, Yap WM, et al. Pancreatic serous oligocystic adenomas: clinicopathologic features and a comparison with serous microcystic adenomas and mucinous cystic neoplasms. *World J Surg*. 2006;30(8):1553-1559. [\[CrossRef\]](#)
24. Yamazaki M, Oyanagi K, Umezu H, et al. Quantitative 3D shape analysis of CT images of thymoma: a comparison With histological types. *AJR Am J Roentgenol*. 2020;214(2):341-347. [\[CrossRef\]](#)
25. Wei S-C, Xu L, Li W-H, et al. Risk stratification in GIST: shape quantification With CT is a predictive factor. *Eur Radiol*. 2020;30(4):1856-1865. [\[CrossRef\]](#)
26. Nioche C, Orlhac F, Boughdad S, et al. LIFEx: a freeware for radiomic feature calculation in multimodality imaging to accelerate advances in the characterization of tumor heterogeneity. *Cancer Res*. 2018;78(16):4786-4789. [\[CrossRef\]](#)
27. Lee JH, Kim JK, Kim TH, et al. MRI features of serous oligocystic adenoma of the pancreas: differentiation from mucinous cystic neoplasm of the pancreas. *Br J Radiol*. 2012;85(1013):571-576. [\[CrossRef\]](#)
28. Elta GH, Enestvedt BK, Sauer BG, Lennon AM. ACG clinical guideline: diagnosis and management of pancreatic cysts. *Am J Gastroenterol*. 2018;113(4):464-479. [\[CrossRef\]](#)
29. European Study Group on Cystic Tumours of the Pancreas. European evidence-based guidelines on pancreatic cystic neoplasms. *Gut*. 2018;67(5):789-804. [\[CrossRef\]](#)
30. Capella C, Solcia E, Kloppel G, Hruban RH. Serous cystic neoplasms of the pancreas. In: Hamilton SR, Aaltonen LA, eds. *World Health Organization Classification of Tumours: Pathology and Genetics of Tumours of the Digestive System*. Lyon: IARC Press; 2000:231-233.
31. Buerke B, Domagk D, Heindel W, Wessling J. Diagnostic and radiological management of cystic pancreatic lesions: important features for radiologists. *Clin Radiol*. 2012;67(8):727-737. [\[CrossRef\]](#)
32. Compagno J, Oertel JE. Mucinous cystic neoplasms of the pancreas with overt and latent malignancy (cystadenocarcinoma and cystadenoma). A clinicopathologic study of 41 cases. *Am J Clin Pathol*. 1978;69(6):573-580. [\[CrossRef\]](#)
33. Zamboni G, Scarpa A, Bogina G, et al. Mucinous cystic tumors of the pancreas: clinicopathological features, prognosis, and relationship to other mucinous cystic tumors. *Am J Surg Pathol*. 1999;23(4):410-422. [\[CrossRef\]](#)
34. Ardakani AA, Gharbali A, Mohammadi A. Classification of benign and malignant thyroid nodules using wavelet texture analysis of sonograms. *J Ultrasound Med*. 2015;34(11):1983-1989. [\[CrossRef\]](#)
35. Li Z, Yu L, Wang X, et al. Diagnostic performance of mammographic texture analysis in the differential diagnosis of benign and malignant breast tumors. *Clin Breast Cancer*. 2018;18(4):e621-e627. [\[CrossRef\]](#)
36. Huang Z, Li M, He D, et al. Two-dimensional texture analysis based on CT images to differentiate pancreatic lymphoma and pancreatic adenocarcinoma: a preliminary study. *Acad Radiol*. 2019;26(8):e189-e195. [\[CrossRef\]](#)
37. Kirienko M, Cozzi L, Rossi A, et al. Ability of FDG PET and CT radiomics features to differentiate between primary and metastatic lung lesions. *Eur J Nucl Med Mol Imaging*. 2018;45(10):1649-1660. [\[CrossRef\]](#)